2017-01-0230

High Strain Rate Mechanical Characterization of Carbon Fiber Reinforced Polymer Composites using Digital Image Correlation

Louise A. Powell, William E. Luecke, Matthias Merzkirch, Katherine Avery and Tim Foecke
Affiliation (Do NOT enter this information. It will be pulled from participant tab in MyTechZone)

Abstract

In order to enable optimal design and manufacturing of vehicle systems, it is important to develop, integrate and implement predictive computational models for carbon fiber polymer (CFRP) composites that link the materials design, molding process and final performance requirements. In this study, dynamic mechanical response of unidirectional (UD) and 2x2 twill weave CRFP composites was characterized at deformation rates applicable to crashworthiness performance. Non-standardized specimen geometries were tested on a standard uniaxial frame and an intermediate-to-high speed dynamic testing frame, equipped with high speed cameras for 3D digital image correlation (DIC). Specimen cross-sections, according to each fiber orientation tested, were consistent across strain rates to ensure results were comparable. Tensile strength and modulus were experimentally investigated over a wide range of strain rates (0.0001 s^{-1} to 200 s^{-1}). DIC was used to estimate strain profiles on composites surfaces, and the modulus was calculated from those strain measurements. Experimental results demonstrated an increase in the tensile strength of UD CFRP composites in the longitudinal (0°) and transverse (90°) direction with increasing strain rates. In contrast, the tensile strength of 2x2 woven composites and the tensile modulus of the UD material were insensitive to increasing strain rates. Comparison of failure modes provided insights on how loading rates influenced failure mechanisms.

Introduction

For the last few decades, carbon fiber reinforced polymer (CFRP) composites have been incorporated in the production of components and structures in aerospace and automotive applications [1,2] due to their high strength capability. Several manufacturers have also substituted metal parts with composites because they can be formed into complex shapes that, for metallic parts, would require machining to create joints. Pre-formed composite components are lightweight and strong and reduce the number of heavy fasteners and joints. Hence, composite materials are helping to drive an industry-wide trend of fewer components, which can contribute towards weight reduction and fuel efficiency increase while being easy to handle, design, shape, and repair.

In the automotive industry, the incorporation of advanced, lightweight materials into vehicle structural components has a mission to save money, energy and reduce emissions.

The design process of automotive structures relies extensively on component level testing to validate the overall component crash performance. However, these tests may not provide sufficient information essential to the development of smarter and more robust modeling tools that link deformation behavior to material characteristics, which are crucial to the design process.

It is necessary for designers to understand the dynamic mechanical characteristics over a broad range of strain rates at a fundamental level in the design process. These characteristics are usually produced from material coupon level testing [3]. Due to the lack of existing standards for high strain rate testing procedures, obtaining accurate dynamic experimental data, suitable for material modeling predictive tools, represents a challenge for current testing methods [3].

Research studies on the effect of strain rates on the mechanical response of CFRP composites have not been fully investigated [4]. A limited amount of data was obtained on the tensile behavior of fiber composites at high strain rates using the expanding ring technique [5, 6]. Techniques used to determine mechanical properties under tensile impact loading of unidirectional (UD) carbon/epoxy and graphite/epoxy composites were investigated [7]; the dynamic stress-strain curves for UD carbon/epoxy and woven fabric glass/epoxy composites were also examined. Tensile tests to determine high tensile strength at various strain rates (crosshead speeds) were conducted [8]. The effect of strain rates via crosshead speeds on tensile strength and Weibull modulus of T1000GB PAN-based carbon fiber epoxy-impregnated bundle composites was evaluated. Nevertheless, the mechanical response of CFRP composites under low and high-speed loading is not entirely understood. In order for tests to generate the required data for building material models and to accelerate new product development, it is necessary to use predictive tools combined with experiments, and integrate them into the full product development cycle. As part of this process, quasi-static and dynamic mechanical characterization of CFRP composite material is currently underway.

The strain rate sensitivity of UD CFRP composites in the longitudinal (0°) and transverse (90°) directions as well as 2x2 twill weave composites at strain rates ranging between 0.0001 s^{-1} to 200 s^{-1} is being characterized in uniaxial tension tests using digital image correlation (DIC). DIC is a non-contact quantitative full-field method to measure displacements in 2D and 3D, and it is capable of quantitative measurement of surface strains during deformation [9]; it is used on the intermediate-to-high speed dynamic testing frame for longitudinal, transverse, and woven strain measurements. A mechanical extensometer is used on specimens tested at lower loading rates on a standard uniaxial testing frame for strain measurements. A specific strain rate of 0.01 s^{-1} ties both testing machines to the same loading rate condition. Also, specimen cross-sections, according to each fiber orientation tested, are consistent across loading rates for comparison purposes. The strain results are used for chord modulus and Poisson's ratio [10] calculations necessary to develop, integrate and implement predictive computational models for CFRPs composites linking the materials design, molding process and final performance requirements for optimal design and manufacturing of CFRP automotive systems. Preliminary results of the stress-strain relationship as well as measured strengths and chord modulus versus a wide range of strain rates are presented in this paper. Comparison of failure modes at different

loading rates is also investigated to determine how loading rates influence specimen failure mechanisms.

Material

Carbon fiber reinforcements, due to their small cross-sections, are not directly used in engineering applications. Therefore, they are embedded in matrix materials to form carbon fiber composites [11]. The matrix serves to bind the fibers together, transfer the loads to the fibers, and protect them from damage due to handling and environmental effects.

The matrix material used in this study was a non-commercialized high temperature cure epoxy resin that was internally supplied by the Dow Chemical company for the purpose of this study. Samples with three types of fiber orientations were produced: carbon fiber reinforced laminate composites with 12-plies of UD fibers in the 0° and 90° directions, as well as carbon fiber reinforced with a 2x2 twill weave laminate composites. The continuous and woven prepregs are produced by DowAksa (A-42 24K) [12], and the composite laminate sheets were formed by the compression molding technique. In this processing method, epoxy/carbon composites were produced with 50:50 volume fraction of fiber/matrix content for the UD material. The 2x2 twill weave laminate has 4-plies with a 50:50 fiber weight ratio in the weft and warp directions.

Non-standardized samples for uniaxial tensile testing were prepared from the composite materials. Figures 1a. and 1b. illustrate the UD specimen geometry and nomenclature, and table 1 shows specimen dimensions. Figures 2a. and 2b. illustrate the 2x2 twill weave specimen geometry, and table 2 shows specimen dimensions.

Specimen Surface preparation

Each specimen in Figures 1a and 2a was cut using abrasive waterjet cutting with fine abrasive of 220 mesh. In order to produce the specimens, the end-tab region of a 250 mm x 250 mm composite panel (UD or woven) subset was abraded using sand paper of 240 grit. The surface of NEMA grade G11 glass reinforced epoxy plastic laminates (yellow material in Figure 1a.) was also abraded in order to roughen the surface to be bonded as tabbing material. The abraded surfaces were washed thoroughly with water and air-dried. Another stage for the surface preparation of end-tabs consisted in using a file to cut a groove in the G11 and placing a wire spacer to control the bondline thickness. Then, the final stage for the surface preparation was to wipe the end-tab areas of the composite panel and the G11 with isopropyl alcohol to get them ready for adhesive bonding [13].

Adhesive Bonding Process

The choice of adhesive for this study was 3M Scotch-Weld Low Odor Acrylic Adhesive DP810 (black) [14]. Curing was conducted in a fume hood at room temperature. The acrylic was dispensed on the G11 and CFRP laminate panels generously. The G11 was then bonded on each side of the CFRP end-tab region and allowed to cure for 24 hours at room temperature. The specimens were cut via waterjet the following day.

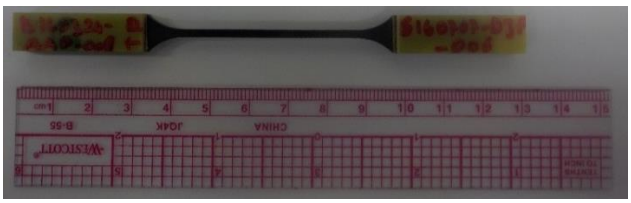

a.

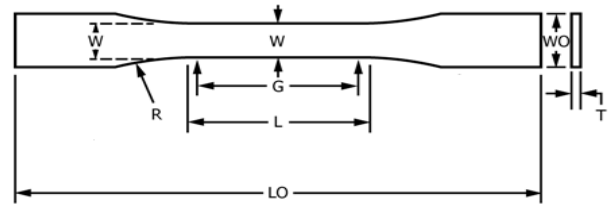

b.

Figure 1. (a) Tensile specimen geometry for unidirectional (UD) material in the 0° and 90°. (b) specimen nomenclature.

a.

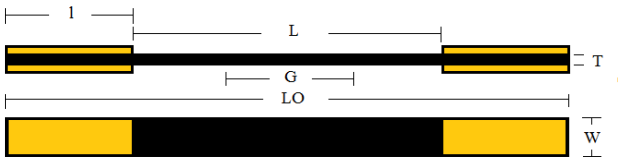

b.

Figure 2. (a) Tensile specimen geometry for 2x2 twill woven laminate composites. (b) specimen nomenclature.

Table 1. UD dogbone specimen dimensions.

Specimen fiber orientation	**Unidirectional (0° and 90°)**
Geometry	Dogbone
LO - Overall length	166 mm
WO - Overall width	9.53 mm
W - Width of narrow section	2.0 mm
T- Thickness of narrow section	2.53 mm
L - Length of narrow section	45.5 mm
G - Reduced gauge length	36.4 mm
R - Radius of fillet	12.7 mm
Tab bevel angle	0°

Table 2. 2x2 twill weave laminate composites rectangular specimen dimensions.

Specimen 2D fabric laminate	**2x2 Twill weave**
Geometry	Rectangular
LO - Overall length	137 mm
W - Width	10.0 mm
T- Thickness	2.73 mm
l - Tab length	38.0 mm
L - Length of parallel section	62.0 mm
G - Reduced gauge length	25.4 mm
Tab bevel angle	0°

Testing Methods

Initially, each UD specimen in the 0° direction, with a shorter gauge length (L = 9.53 mm or geometry type I), was tested individually on a servohydraulic test machine with a 50 kN load cell capacity. An extensometer was used for strain measurements. The extensometer had a gauge length of G = 8.6 mm and was calibrated in units of strain. Uniaxial tensile tests were conducted with the displacement rate programmed for each test to provide engineering plastic strain rates nominally 0.0001 s^{-1}, 0.01 s^{-1} and 0.5 s^{-1}.
A second set of specimens with L = 45.5 mm (or geometry type II) were individually tested on a high strain rate (HSR) servohydraulic test machine with a 12 kN load cell capacity. These specimens were modified from the previous in terms of a longer gauge to accommodate their placement for subsequent tests conducted on the HSR machine.

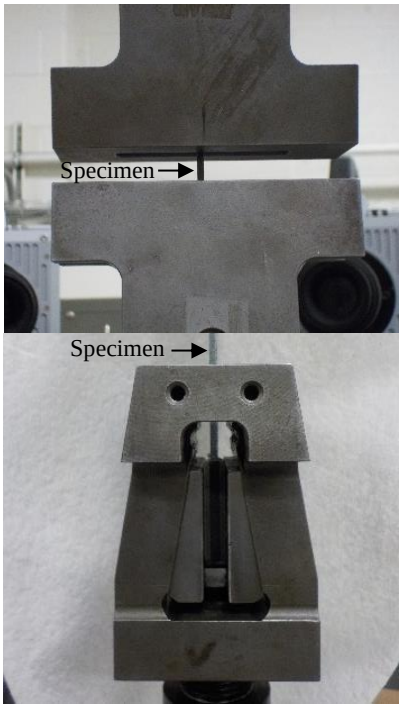

Figure 3. High-strain rate (HSR) wedge-grip system (front and side views).

Surface Strain Measurements

On the HSR testing machine, strain measurements were collected using high-speed DIC cameras and acquisition system. DIC is capable of quantitative measurement of severe surface strain gradients at a close location, hence representing high spatial resolution [15]. DIC working principles have been explained in [15-16]. In this study, the high-speed DIC cameras are Photron Fastcam SA5 and are used in combination with 200 mm Nikon lenses with locking focus rings and apertures. The DIC cameras were mounted to a continuous aluminum bar to warrant that their spacing and orientation remained unchanged during each experiment. The setup with a specimen mounted in the HSR grips is shown in Figures 3 and 4.
In order to capture surface strain measurements using DIC methods, digital images before and after deformation and displacement of small subsets of the area of interest are compared. The tracing process is possible when observed surface has speckle patterns, which in the case of the presented results, was obtained by manually spraying matte white primer base paint on the specimen and matte black paint for speckle patterns (≈50/50 black/white) as shown in Figure 5. When applying speckle patterns, each rectangular subset of a few pixels has a unique distribution of grey level. The system was calibrated by acquiring grid images using a 14x10 target (grid) with a 3 mm pitch.

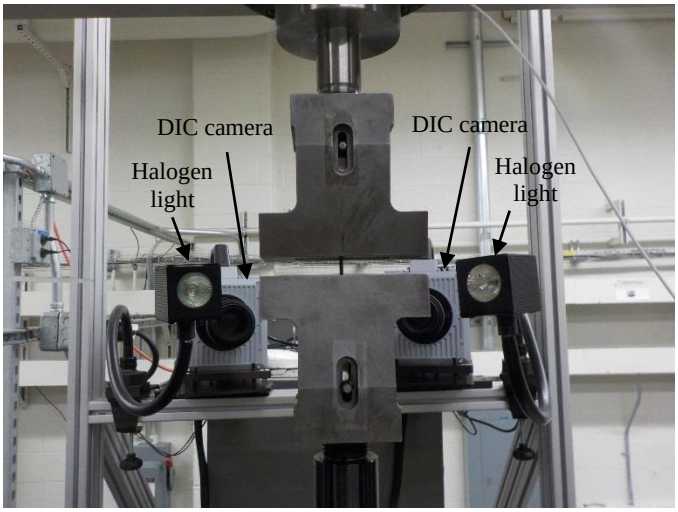

Figure 4. HSR setup with DIC cameras and halogen lighting system.

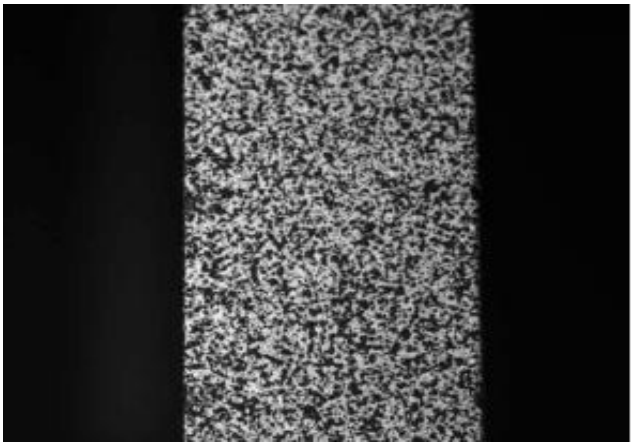
Figure 5. DIC matte white base paint and black speckle patterns on CFRP specimens.

Data Acquisition

The high-rate system has two parallel data acquisition units. Vic-Snap drives a National Instrument USB DAQ (NI USB6221) that reads up to 21 000 frames per second. All the signals are delivered in parallel to the analog inputs of both DAQs via BNC-tee connections. The high-rate DAQ is also triggered by the signal from the "fire-control" button, which triggers the cameras as well.

Results and Discussion

Stress and Strain Calculated from Experiments

CFRP specimens with fiber reinforcements in the 0° direction tested on the servohydraulic testing machine were equipped with an extensometer. The engineering strains in the stress-strain curves in Figure 6 were mathematically shifted so that the extrapolation of the elastic modulus line intersects the origin. The engineering strain rate

was calculated by fitting a spline to the strain-time data before the first fiber break and evaluating the first derivative of the spline.
The nominal strain rate reported is calculated from the commanded actuator velocity divided by the length of the reduced parallel length, L. Figure 6 shows engineering stress-strain curves of the tensile tests at quasi-static rate of 0.0001 s^{-1}. Specimens with shorter gauge lengths (L = 9.53 mm) were limited to three (3) tests per rate condition. Interestingly, the first set of fiber breakage occurred at the same stress (855 ± 65 MPa) for all three rates of 0.0001 s^{-1}, 0.01 s^{-1}, and 0.5 s^{-1}. This breakage was recorded by specimens instrumented with the extensometer. the nominal elastic modulus was calculated by linear regression to the engineering stress-strain data in the range of 0.001 to 0.003 absolute strain [10].
The experimental stress–strain curves in this study are based on the total strain on the gauge length of the specimen. The stress is the axial force recorded by the load cell divided by the initial cross-section of the specimen. The stress and strain recorded at the peak of the stress versus strain curves are the specimen ultimate tensile strength and strain [10]. Figure 7 shows that UD (0°) CFRP specimens ultimate tensile strengths increase as a function of increasing strain rates. Table 3 shows a summary of results for specimens with a shorter gauge length (L = 9.53 mm).

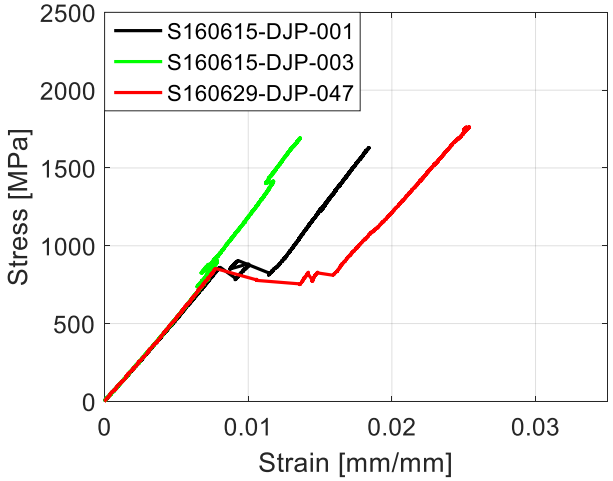

Figure 6. Stress-strain relationship for UD (0°) CFRP specimens all tested at 0.0001 s^{-1}. These curves show fiber breakage occurring at the same stress (855 ± 65 MPa).

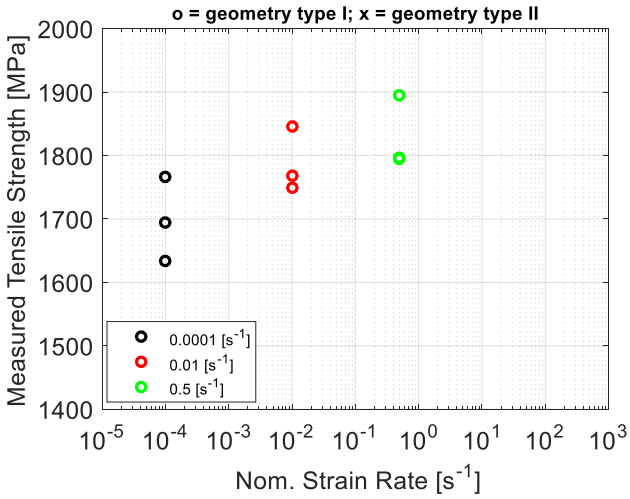

Figure 7. Measured ultimate tensile strengths for all three rates for UD (0°) CFRP specimens with a shorter gauge length (L = 9.53 mm).

UD (0°) CFRP specimens were tested on the HSR servohydraulic testing machine. Specimens with a longer gauge length (L = 45.5 mm), were limited to 3 tests per rate condition. All four testing conditions were 0.01 s^{-1}, (which ties both testing machines to the same rate condition), 1 s^{-1}, 10 s^{-1} and 200 s^{-1}. The nominal strain rate reported was also calculated from the commanded actuator velocity divided by the length of the reduced parallel length, L.
Figure 8 shows the measured elastic modulus as a function of nominal strain rate. A linear regression (not reported) provided no indication that the modulus depended on strain rate.

Table 3. Mechanical properties of UD (0°) CFRP specimens with a shorter gauge length (L = 9.53 mm).

Nom. strain rate [S^{-1}]	**Measured Modulus [GPa], (CoV %)**	**Ultimate Tensile Strength [MPa], (CoV%)**
0.0001	108.2 (1.9 %)	1698 (3.8 %)
0.01	109.8 (4.4 %)	1787 (2.8 %)
0.5	108.9 (2.4 %)	1828 (3.1 %)

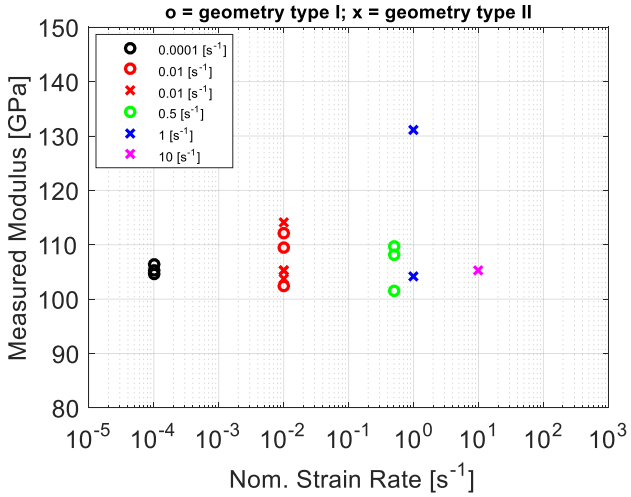

Figure 8. Measured modulus. Geometry type I are the shorter gauge length (L = 9.53 mm) specimens and geometry type II are the longer gauge length (L = 45.5 mm) specimens.

Transverse specimens (with fibers in the 90° orientation) were tested at three (3) strain rates: 0.01 s^{-1}, 1 s^{-1} and 200 s^{-1} on the HSR servohydraulic testing machine. The specimens tested had a longer gauge length (L = 45.5 mm).
The DIC measured positions and displacements are rotated to a user defined orthogonal (x, y, z) coordinate system, which is based on reference marks located at the center of the specimen that were made during patterning. The positions x, y, and z are in reference to the selected coordinate system. The x-positive axis follows the north vertical direction from the center point of the specimen gauge length. The y-positive axis follows the west horizontal direction from the center point of the specimen gauge length. The z-positive axis is toward the DIC camera system. A color map on a scale of 2 % strain with a transition from colors pink (lower strain values of 0.05 % strain) to red (higher strain values of 2 % strain) was used on the DIC images illustrating the axial strain, e_{xx} in the x-direction (loading direction) for the transverse specimen tested at high-rate of 200 s^{-1}. These results are shown as contour plots of strain that overlay the image at the current

stage of loading in Figure 9. Figure 9a shows the specimen before failure, Figure 9b shows strain localization at specimen failure.

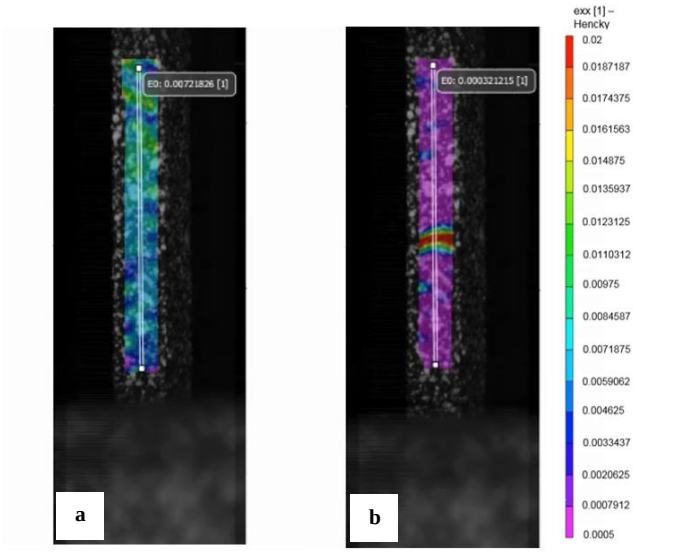

Figure 9: DIC contour plots of axial strain pre-failure (a) and at failure (b) for a transverse specimen tested at 200 s^{-1}.

A visual extensometer tool from the VIC 3D analysis software was also used to calculate the engineering strain, which was obtained from the amount of deformation in the loading direction divided by the initial length of the material,

$$\varepsilon = \frac{\Delta L}{L}, \text{ with } \Delta L = L' - L \quad (1)$$

where L is the initial length of the specimen, L′ is the new length, and $\Delta \mathbf{L}$ is the change in length.

Results show that ultimate tensile strengths of transverse specimens (90°) are strain rate sensitive as illustrated in Figure 10. There is an increase of 37 % in specimen strength as the strain rate increases from 0.01 s^{-1} to 200 s^{-1}.

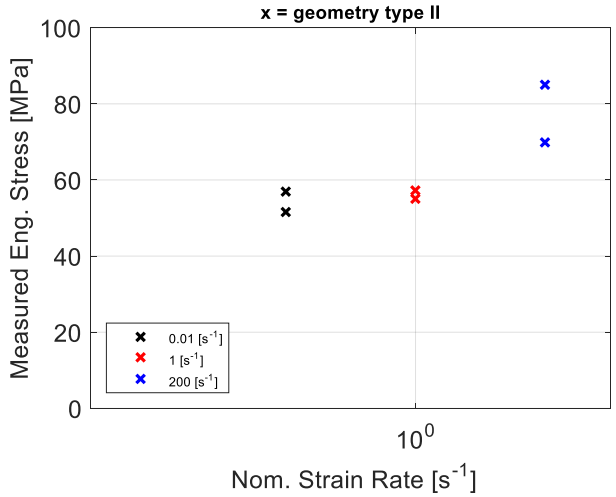

Figure 10. Ultimate tensile strengths on the HSR machine for UD (90°) CFRP specimens with a L = 45.5 mm.

Preliminary tensile tests were conducted on the CFRP 2x2 twill weave material. For this material, each weft roving passes over and under two warp rovings; similarly, each warp roving passes over and under two weft rovings. Each specimen was axially loaded in the warp direction. Specimens tested at strain rates 0.0001 s^{-1} and 0.01 s^{-1} were equipped with a mechanical extensometer with a gauge length of 24.5 mm. The specimen dimensions are shown in Table 2.

Although more specimens are currently being tested at those intermediate rates to ensure repeatability of results, measured ultimate tensile strengths of woven specimens are not sensitive to strain rate based on the current data (within 0.0001 s^{-1} to 1 s^{-1}) as shown in Figure 11.

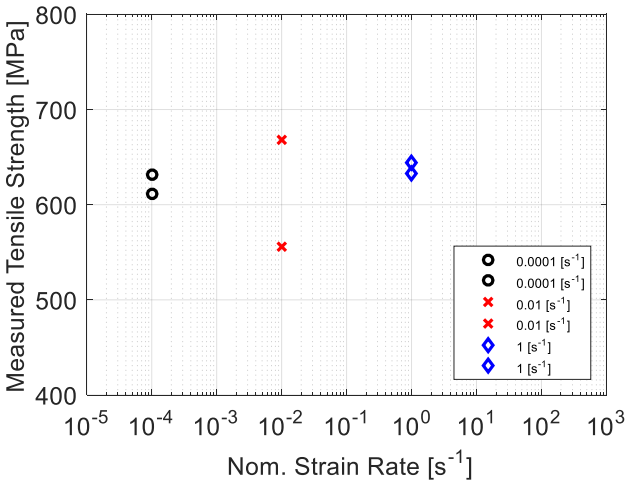

Figure 11. Measured ultimate tensile strengths for CFRP 2x2 twill weave specimens.

Additional testing is currently ongoing for CFRP 2x2 twill weave for characterizing the mechanical properties over a wider range of loading rates (0.01 s^{-1}, 1 s^{-1}, 10 s^{-1}, and 200 s^{-1}) on the HSR machine using DIC. The fiber reinforced textile architecture affects the generation of strain localizations, which can contribute to a possible increase in crack propagation in the specimen.

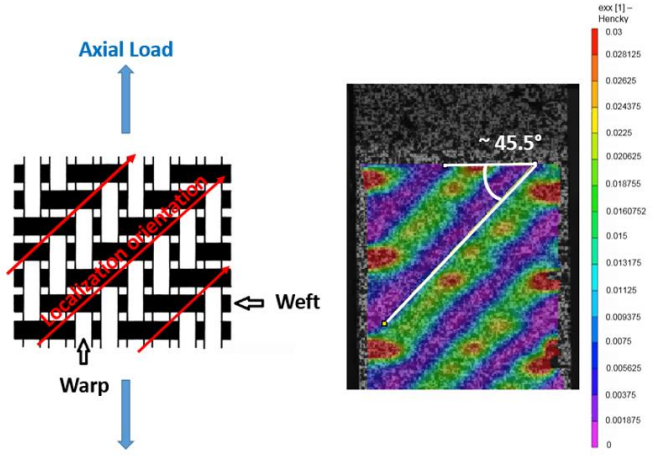

a. b.

Figure 12. a. 2D fabric orientation in a CFRP 2x2 twill weave laminate specimen. b. DIC contour plot of axial strain, e_{xx} as delamination occurs. Strain localizations are oriented at 45.5°.

During tensile testing of the woven material, the specimen, loaded axially in the warp direction (Figure 12a.), exhibits numerous cracks that are also audible due to delamination occurring in the specimen. Strain localizations, oriented in the 45° direction for images registered just after delamination are presented as a contour plot of strain that overlays the image at the current stage of loading in Figure 12b. A color map on a scale of 3 % strain with a transition from colors pink to

red is used on the DIC image illustrating the axial strain, e_{xx} in the x-direction (loading direction) for a woven specimen tested at an intermediate rate of 0.01 s^{-1}. As shown in Figure 12, these strain localizations occurred around the fiber tow intersections or woven material crimps and are oriented at about 45.5°. Specimen failure tends to initiate at the crimps as well. Table 4 shows preliminary results for CFRP 2x2 twill weave laminate specimens tested on the servohydraulic machine.

Table 4. Mechanical properties of CFRP 2x2 twill weave laminates composites tested on the servohydraulic machine.

Nom. strain rate [1/s]	**Measured Modulus [GPa], (CoV %)**	**Ultimate Tensile Strength [MPa], (CoV%)**
0.0001	59.3 (2.4 %)	621.5 (2.3 %)
0.01	56.4 (1.1 %)	611.9 (13.0 %)
1	-	639.0 (1.3 %)

Fractography

This section describes fractographic features observed in all CRFP specimens tested in tension and at the different loading rates investigated.

UD CFRP specimens in the 0° direction showed different modes of failure for shorter gauge length specimens when compared to longer gauge length specimens (Figure 13). Acceptable failures showed that specimens with shorter gauge lengths (L = 9.53 mm) failed by lateral, gauge, middle (LGM) and lateral, gauge, bottom (LIB) failure codes [10]. All acceptable failures for specimens with longer gauge lengths (L = 45.5 mm) failed by long-splitting, gauge, various (SGV) and lateral, gauge, bottom (LIB) failure codes [10]. A visualization of tensile test failure codes and typical modes is shown in Figure 14.

UD CFRP (with fibers oriented in the 90° direction) failed specimens showed different modes when tested on the HSR machine. Acceptable failure modes varied depending on the strain rate condition. Figure 15 shows that specimens tested at lower strain rates failed with a single break, and specimens tested at higher rates had multiple breaks along the gauge length.

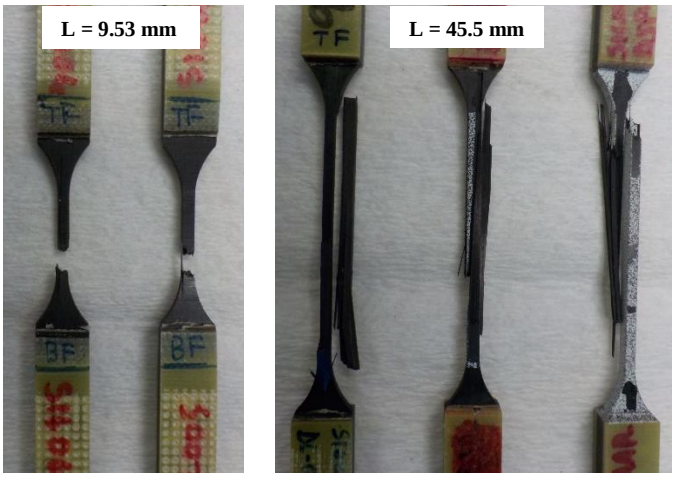

Figure 13. Failure modes for UD CFRP specimens with fibers oriented in the 0° direction with shorter and longer gauge lengths at 0.01 s^{-1}.

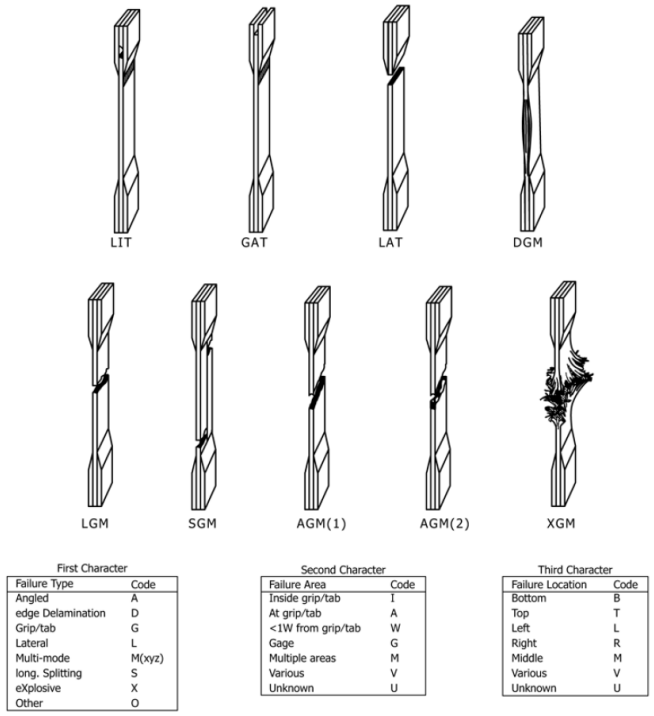

Figure 14. Tensile test failure codes and typical modes for polymer matrix composite materials [10].

Figure 16 shows DIC images of a transverse specimen tested at a strain rate of 200 s^{-1}. The second break appeared on the specimen in the last two images after the first break. These second breaks were attributed to the release of elastic energy during specimen failure, which propagated into the specimen gauge length after the actuator engaged (post-test).

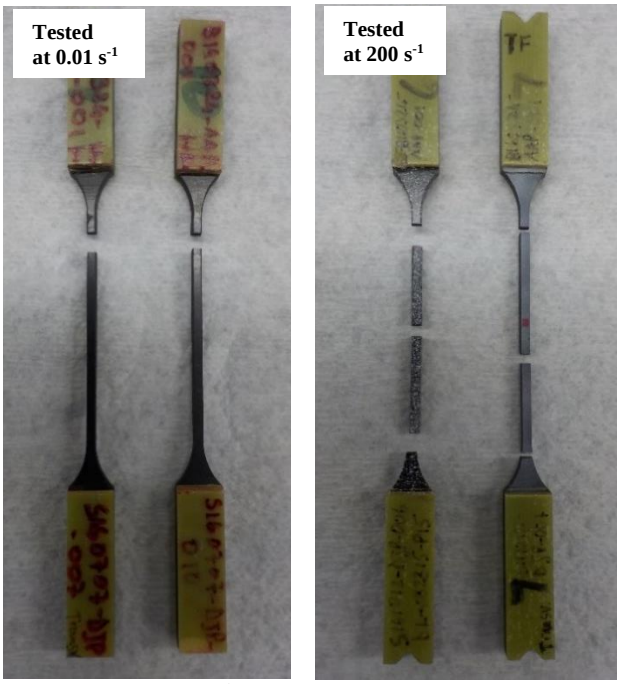

Figure 15. Failure modes for UD [90°] CFRP specimens with longer gauge lengths.

The types of failure codes reported were lateral, gauge, top (LGT) for specimens that were tested at lower intermediate rates of 0.01 s^{-1}, and lateral, gauge, various (LGV) for specimens that were tested at high strain rates of 200 s^{-1}. At strain rates of 1 s^{-1} the failure code was either LGT or LGV.

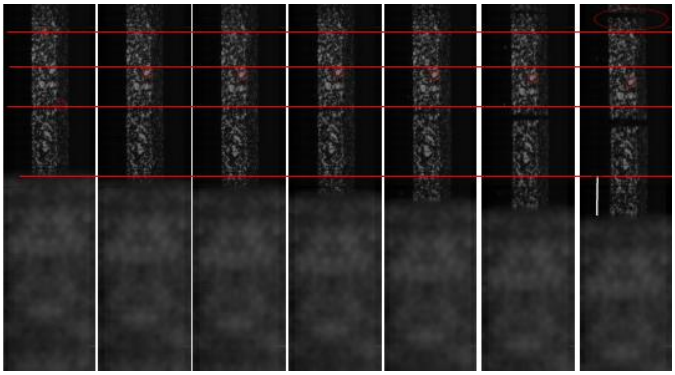

Figure 16. UD (90°) CFRP transverse specimens with a longer gauge length (L = 45.5 mm) tested on the HSR machine with high-speed DIC camera at 200 s^{-1}. The time between each frame was 25 µs.

Tensile tested UD specimens in the transverse direction (fibers in the 90° orientation) showed matrix cracking types of failure at intermediate strain rates (i.e.: 0.01 s^{-1}) and extensive matrix damage at high strain rates (i.e.: 200 s^{-1}). The failure of UD transverse specimens is matrix dominant as shown in left images of Figures 17 and 18. It is important to note that at high strain rates of 200 s^{-1}, there was an increase in small groups of fibers breaking across the fractured surface (right image of Fig. 18). Those breaks were not observed on tensile specimens fractured surfaces at lower strain rates (0.01 s^{-1}) as seen on the right image of Fig. 17. This increase in groups of fiber breaks may contribute to an increase in specimen failure strengths, which was noticed at high-rate tensile tests in Fig. 10.

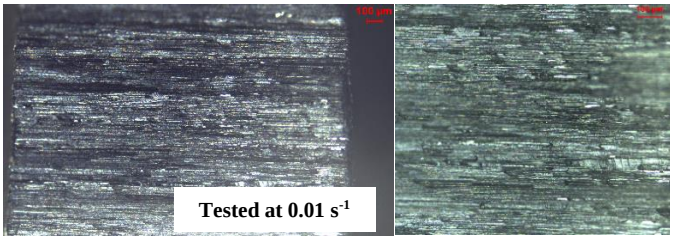

Figure 17. Micrographs of cross-sectional views for the tensile fractured surfaces of UD (90°) CFRP specimens with longer gauge lengths at a strain rate of 0.01 s^{-1} (the magnification is 50 on the left and 100 on the right).

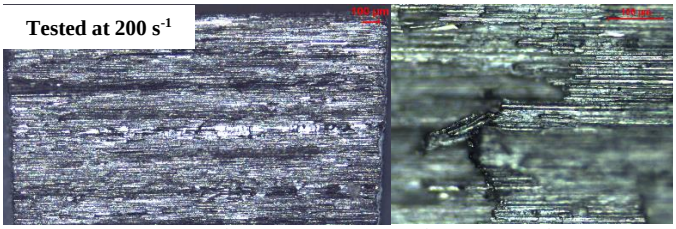

Figure 18. Micrographs of cross-sectional views for the tensile fractured surfaces of UD (90°) CFRP specimens with longer gauge lengths at a strain rate of 200 s^{-1} (the magnification is 50 on the left and 200 on the right).

Tensile tested specimens of CFRP 2x2 twill weave material showed similar failure modes at all tested strain rates (0.0001 s^{-1}, 0.01 s^{-1} and 1 s^{-1}). Figure 19 shows significant delamination within the laminates, and micrographs illustrate matrix dominated fractures in the weft rovings (Figure 20).

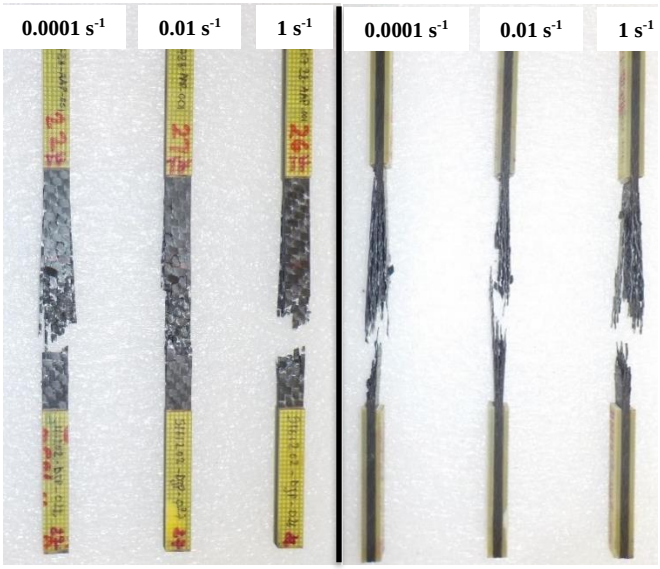

Figure 19. Specimens failure modes for CFRP 2x2 twill weave specimens.

As shown in Figure 19, major delamination was visible on each specimen at all tested rates. In addition, cracks, which were noticeable along the length of the specimen, also ran from one side to the other across the specimen width as shown in the micrographs of Figure 20. Failure initiated in the resin rich regions around the tow intersection (at the crimp location) and propagated in those regions. In turn, since the failure in the woven material was mostly matrix dominated, the strength of the material did not demonstrate an increase as strain rates increased from 0.0001 s^{-1} to 1 s^{-1} (Figure 11) based on current data.

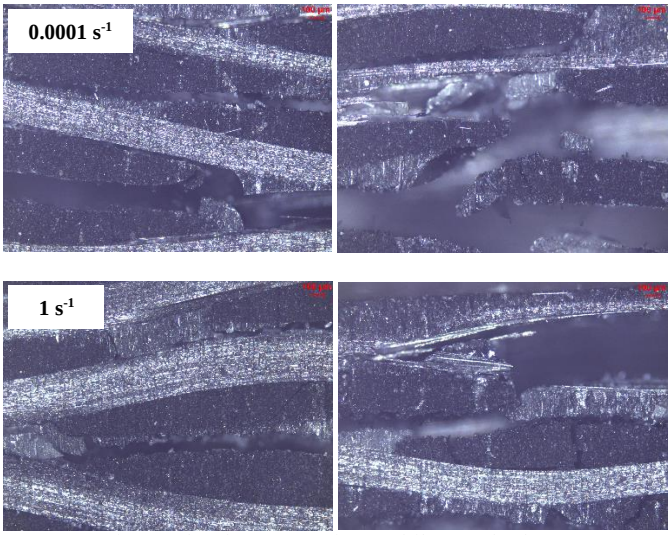

Figure 20. Micrographs of woven specimens' failure modes for CFRP 2x2 twill weave specimens. Specimen tested at 0.0001 s^{-1} is shown in the top two micrographs and specimen tested at 1 s^{-1} is shown in the bottom two micrographs. Micrograph views are in the weft direction from the edge of the specimen.

Conclusions

In order to enable optimal design and manufacturing of vehicle systems through the process of developing, integrating and implementing predictive computational models for carbon fiber reinforced polymer (CFRP) composites that relate the materials design, molding process and final performance requirements, the

mechanical properties and failure mechanisms occurring in structural components over a wide range of loading rates have been assessed in this ongoing study. CFRP composite with three different fiber orientations: unidirectional (UD) materials in the 0° and 90° and woven 2x2 twill composites were tested.

Tensile tests were performed on a standard uniaxial testing frame and an intermediate-to-high speed dynamic testing frame, equipped with high speed cameras for 3D digital image correlation (DIC). Strain rates of interests ranging between 0.0001 s^{-1} to 200 s^{-1} were investigated on non-standardized specimen geometries. Specimen cross-sections, given a fiber orientation, were consistent across strain rates to ensure results were comparable.

Preliminary UD CFRP composites specimens tested showed an increase in the ultimate tensile strengths with increasing strain rates on both servohydraulic systems. Specimen strengths with fibers in the longitudinal direction increased by 8 % and specimens with fibers in the transverse direction by 37 %. In contrast, CFRP 2x2 twill woven composites specimen strengths were insensitive to increasing strain rates. In addition, analysis of the experimental local strain data showed that measured tensile chord modulus seemed independent of strain rates for UD CFRPs in the 0° orientation.

Failure modes gave consistent acceptable failure codes for specimens in the 0° orientation for all systems, but the length of the gauge had an effect on failure modes. All specimens with a shorter gauge length had lateral gauge failures; meanwhile, all specimens with a longer gauge length had long-splitting types of failures.

UD transverse (90°) specimens had failure breaks that were strain rate dependent. All specimens tested at low loading rates had a single break, and other specimens tested at higher high loading rates had multiple breaks in their gauge section. Additional breaks in the gauge section were attributed to the release of elastic energy during specimen failure.

Finally, CFRP 2x2 twill woven specimens DIC images, presented as contour plots showed strain localizations, oriented in the 45.5° direction, for images registered just after delamination. Thus, the architecture of 2D fabric reinforcements (2x2 twill weave in the lamina) affected the strain localization direction, which may have contributed to an increase in cracks propagation in the specimen resin rich regions.

Additional testing is currently ongoing for all materials to completely characterize the mechanical properties over the defined wide range of loading rates with DIC.

References

1. Fitxer, E., “PAN-Based Carbon Fibers: Present State and Trend of the Technology from the Viewpoint of Possibilities and Limits to Influence and to Control the Fiber Properties by the Process Parameters,” *Carbon*, 27(5):621–645, 1989, doi: 10.1016/0008-6223(89)90197-8.
2. Fitxer, E. and Heine, M., “in Fiber Reinforcements for Composite Myers: Composite Material Series,” vol. 2, ed. by A. R. Bunsell, Elsevier Publishers, Amsterdam, 1988, pp. 73-148.
3. Olivares, G., Acosta, J.F., Yadav, V., Keshavarayana, S., and Abramowitz, A., “Crashworthiness of Composites – Certification by Analysis,” FAA JAMS 2011 Technical Review Meeting, Apr. 2011.
4. Gilat, A., Goldberg, R. K., and Roberts, G. D., “Experimental Study of Strain-Rate-Dependent Behavior of Carbon/Epoxy Composite,” *Compos. Sci. Technol.*, 56(7):1469–1476, 2002, doi:10.1016/S0266-3538(02)00100-8.
5. Daniel, I. M., LaBedz, R. H., and Liber, T., "New Method for Testing Composites at Very High Strain Rates," Experimental Mechanics, 21(2):71-77, 1981, doi:10.1007/BF02325199.
6. Daniel, I., Hamilton, W., and LaBedz, R., "Strain Rate Characterization of Unidirectional Graphite/Epoxy Composite," Composite Materials: Testing and Design (6th Conference), STP28492S, I. Daniel, Ed., ASTM International, West Conshohocken, PA, 1982, pp. 393-413, doi:10.1520/STP28492S.
7. Harding, J. and Welsh, L. M., “A tensile technique for fiber - reinforced composites at impact rates of strain,” *J. Mater. Sci.* 18(6):1810-1826, 1983, doi:10.1007/BF00542078.
8. Naito, K., “Effect of Strain Rate on Tensile Properties of Carbon Fiber Epoxy-Impregnated Bundle Composite,” *J. of Materi. Eng. Perform.* 23(3):708-714, 2014, doi:10.1007/s11665-013-0823-5.
9. Daggumati, S., Voet, E., Van Paepegem, W., et al., “Local Strain in a 5-Harness Satin Weave Composites under Static tension: Part I – Experimental Analysis,” *Compos. Sci. Tech.* 71:1171-1179, 2011, doi:10.1016/j.compscitech.2011.03.021.
10. ASTM D3039, “Standard Test Method for Tensile Properties of Polymer Matrix Composite Materials,” ASTM International, 100 Barr Harbor Drive, PO Box C700, West Conshohocken, PA 19428-2959.
11. Agarwal, B.D., Broutman, L.J., and Chandrashekhara, K., “Analysis and Performance of Fiber Composites, 3rd Edition., John Wiley & Sons, Inc, New Jersey, 2006.
12. DowAksa, “24K A-42 Technical Data Sheet,” Feb. 2016, Accessed Jan. 22, 2017, http://www.dowaksa.com/wp-content/uploads/2016/03/24K-A-42.pdf.
13. Adams, D.O. and Adams, D.F., “Tabbing Guide for Composite Test Specimens,” *Federal Aviation Admin. Report No. DOT/FAA/AR-02/106*, October 2002, Accessed Jan. 22, 2017, http://www.tc.faa.gov/its/worldpac/techrpt/ar02-106.pdf.
14. 3M, “Scotch-Weld™ Low Odor Acrylic Adhesive DP810 Black Technical Data Sheet,” Apr. 2016, Accessed Jan. 22, 2017, http://multimedia.3m.com/mws/media/66280O/3m-scotch-weld-low-odor-acrylic-adhesives.pdf.
15. Anzelotti, G., Nicoletto, G., and Riva, E., "Mesomechanic Strain Analysis of Twill-Weave Composite Lamina under Unidirectional In-Plane Tension," *Composites Part A: Applied Science and Manufacturing*, 39(8):1294-1301, 2008, doi:10.1016/j.compositesa.2008.01.006.
16. Takanoa, N., Zakoa, M., Fujitsua, R., and Nishiyabub, K., "Study on large deformation characteristics of knitted fabric reinforced thermoplastic composites at forming temperature by digital image-based strain measurement technique," *Compos. Sci. Tech.* 64(13-14):2153-2163, 2004, doi:10.1016/j.compscitech.2004.03.016.

Contact Information

Corresponding author Tel. (301) 975-2415.
E-mail address: louise.ahurepowell@nist.gov (L. Ahure Powell)

Acknowledgments

This work was carried out under the ICME Development of Carbon Fiber Composites for Lightweight Vehicles project directed by Ford and funded by the U.S. Department of Energy under contract number DE-EE0006867. The authors thank David Pitchure for waterjet cutting all specimens tested in this study.

Definitions/Abbreviations

CFRP	Carbon fiber reinforced polymer
HSR	High strain rate
DIC	Digital image correlation
UD	Unidirectional

Disclaimer

Certain commercial equipment, instruments, or materials are identified in this paper to foster understanding. Such identification does not imply recommendation or endorsement by the National Institute of Standards and Technology.